Research Paper

Aromatic heterocycle-grafted NH$_2$-MIL-125(Ti) via conjugated linker with enhanced photocatalytic activity for selective oxidation of alcohols under visible light

Zhenyu Wu, Xiubing Huang[*], Haiyan Zheng, Peng Wang, Guangtong Hai, Wenjun Dong, Ge Wang[*]

Beijing Key Laboratory of Function Materials for Molecule & Structure Construction, School of Materials Science and Engineering, University of Science and Technology Beijing, Beijing, 100083, China

ARTICLE INFO

ABSTRACT

A novel and facile post-grafting strategy, via a Schiff base chemical reaction between aldehyde and $-$NH$_2$ groups within NH$_2$-MIL-125(Ti) has been developed to construct aromatic heterocycle-grafted metal organic frameworks (MOFs) photocatalysts. The improved conjugated system in MOFs showed lower band gaps and their excellent catalytic activities were manifested by selective oxidation of alcohols to corresponding aldehydes under visible light irradiation with high conversion and selectivity. Density functional theory (DFT) was applied for simulating the band gaps and electron orbits of heterocycle-grafted MOFs. The post-synthetic aromatic heterocycles in the MOFs network did not influence the original framework, but effectively expanded its π-delocalized system and promoted the separation and transfer of photo-excited charge carriers. As a result, the aromatic heterocycle-grafted MOFs exhibit significantly enhanced visible-light photo-catalytic activity for selective oxidation of alcohols over pristine NH$_2$-MIL-125(Ti). Especially, the NH$_2$-MIL-125(Ti) grafted by 2-quinolinecarboxaldehyde and 3-thiophenecarboxaldehyde showed better performance (more than 85% conversion of benzyl alcohol) due to the excellent photon adsorption and charge carriers transfer of aromatic heterocycles grafted on MOFs. This general grafting strategy can be utilized to graft large numbers of aromatic rings with different molecular structures onto NH$_2$-MIL-125(Ti).

1. Introduction

Metal organic frameworks (MOFs) are crystalline porous solids with high surface areas and highly tunable properties [1]. At present, a large number of MOF materials have been synthesized [2–5], mainly containing organic carboxylate anion ligands, or nitrogen-containing hetero-cyclic organic neutral ligands. Most of these MOFs have high specific surface areas with relatively stable chemical structures. The pore structure can be tuned, and the specific surface area can reach about 5000 m^{2}g^{-1} [6–9], which is much more advanced than the traditional photo-catalytic materials such as TiO$_2$ [10].

The rapid development of photocatalysis technology has provided a possibility for mankind to explore a green and sustainable development path. After several decades of research, various types of photocatalytic materials have been used. The mechanism of the excitation and charge transition in MOFs is similar to that in the traditional semiconductors [11]. Each metal site in the MOF material can be regarded as an inorganic semiconductor quantum dot, and the ligand in MOF plays a role

in stimulating and conducting charge carriers. Therefore, by modulating the ligands and metals, it is highly feasible to obtain photo-catalytic materials with high visible light response [12,13]. Moreover, since the photochemical reactions occurring in MOFs tend to be confined to their narrow channels, the migration and diffusion length of photo-generated charge carriers can be greatly shortened and the catalytic reaction can be promoted rapidly [14–16]. Finally, the topological structure of the MOFs determines that the active sites are well dispersed and do not easily agglomerate thus the catalyst can maintain excellent stability and long-term performance. Therefore, compared with the traditional semiconductor photocatalysts, the structural advantages of MOFs in photo-induced electron conduction guarantee the most promising research and applications of photocatalytic materials.

Benzaldehyde, an important fine chemical raw material and intermediate, is widely used in imine, benzoyl benzene and other synthetics [17,18]. Since its unique aromatic odor, benzaldehyde is also used extensively for the synthesis of fragrances and spices. At present, there are numerous studies on the green synthesis of aromatic acids in

academia. In view of the fact that photocatalytic technology has an environmentally friendly and sustainable advantage, the photocatalytic oxidation is considered to be a more reliable and promising green synthesis technology. Because MOFs themselves have high specific surface areas and stable performance, they have been widely used in the selective oxidation of benzyl alcohol research. Remarkably, the progress on MOFs serving as oxidation catalysts has been summarized in a comprehensive review on selective or chiral oxidation catalyst [19], however most of the studies describe the loading of Au or Pt nanoparticles on MOFs. Although the noble metal nanoparticles have excellent activity and selectivity, it is a difficult way to produce benzaldehyde on a large scale due to the leak of the nanoparticles and the expensive cost. Therefore, it is necessary to develop a green, highly selective, and environmentally friendly approach to produce benzaldehyde under moderate conditions with MOFs. The post-synthetic modification (PSM) of MOFs is a viable route of synthesizing functionalized MOFs and generating multiple active sites [20–22]. Maxim A. Nasalevich et al. modified NH$_2$-MIL-125(Ti) with dye-like molecular fragments, which showed better light adsorption capacity than that of NH$_2$-MIL-125(Ti) in the visible light range [23]. Jing Xiao et al. introduced salicylaldehyde into NH$_2$-MIL-101(Cr) and enhanced the light-absorption of aromatic heterocycle-grafted NH$_2$-MIL-101(Cr), and showed excellent photodegradation efficiency of methylene blue under the visible-light irradiation [24]. It is also revealed that the introduction of the conjugated structure could improve the efficiency of photocatalyst to a certain extent [25–28].

In this work, Ti-based NH$_2$-MIL-125(Ti) was prepared by a hydrothermal method, and various aldehydes such as pyridine-4-carboxaldehyde were reacted with amino groups in NH$_2$-MIL-125(Ti), as shown in Scheme 1 [29–31]. The new materials were synthesized by means of post-synthetic grafting and were expected to improve the oxidation efficiency of alcohols. In order to reveal the mechanism of synergetic enhancement in catalytic materials, and to explore the effective integration and promotion of catalytic function, the band gaps of specific area in MOFs were computed at the HSE06 level of theory, and the band gaps of MOFs were calculated from UV–vis DRS spectra. Finally, the relationship between the band gap and the specific catalytic performance was verified by experiments.

2. Experimental section

2.1. Catalyst preparation

The synthesis of NH$_2$-MIL-125(Ti) was carried out as reported previously [32]. The synthesized NH$_2$-MIL-125(Ti) was pretreated in a vacuum oven (120 °C) for about 3 h to remove residual water and small organic molecules in the catalyst before the post-synthetic grafting. In a typical synthesis, 280 mg activated NH$_2$-MIL-125(Ti) was transferred

into 25 ml round-bottomed flask, then 15 ml of anhydrous acetonitrile and 0.4 mmol of 2-pyridinecarboxaldehyde (2-PA) were added to the flask. The reaction system was placed in an oil bath at 70 °C with stirring for 3 days. After completion of the reaction, the dark yellow suspension was centrifuged and washed three times with methanol and dried in a vacuum oven at 60 °C overnight, to finally obtain the yellow 2-PA-MIL-125(Ti). Using the same method, 3-pyridinecarboxaldehyde (3-PA), 4-pyridinecarboxaldehyde (4-PA), 3-thiophenecarboxaldehyde (THI), 2-quinolinecarboxaldehyde (QUI) was modified on NH$_2$-MIL-125(Ti) and named as 3-PA-MIL-125(Ti), 4-PA-MIL-125(Ti), THI-MIL-125(Ti), QUI-MIL-125(Ti), respectively. The reaction time was fixed at 3 days in order to modify the respective aldehydes onto NH$_2$-MIL-125(Ti) under the same reaction conditions. The chemical equilibrium of each reactant is controlled in the same state.

2.2. Catalyst characterization

X-ray diffraction (XRD) was conducted using a M21X diffractometer operated at 40 kV and 200 mA with Ni-filtered Cu Kα irradiation (λ = 1.541 Å) source. XRD patterns were scanned over the angular range of 5 − 30° (2θ) with a step size of 0.02°. Fourier transform infrared spectra (FT-IR) were measured by a Nicolet 6700 spectrometer. Porosity and Brunauer-Emmett-Teller (BET) surface area were measured by an AUTOSORB-1C analyzer. After the sample was degassed in a vacuum at 150 °C for 10 h, the nitrogen adsorption and desorption isotherms were measured at −196 °C. The pore volumes and pore size distributions were derived from the adsorption branches of isotherms by using the Barrett–Joyner–Halenda (BJH) model. UV–vis diffuse reflectance spectra (DRS) were recorded on a Shimadzu UV-2550. Barium sulphate (BaSO$_4$) was used as a reflectance standard. ^{1}H NMR was analyzed by Varian UnityPlus 400 after the modified MOFs were digested in DMSO-d^6 respectively. Mott-Schottky analysis was performed at a Princeton electrochemical workstation, it was carried out on the ITO at a frequency of 2 kHz. The counter electrode was a Pt plate, and the potentials were measured against Ag/AgCl in saturated Na$_2$SO$_4$. Fluoromax-4 spectrophotometer was used to obtain photolumine-scence (PL) spectra

2.3. Catalytic tests

The photocatalytic alcohols oxidation was performed in a sealed reaction tube pre-saturated with O$_2$ atmosphere under visible light irradiations. The photocatalyst (30 mg) suspended in solvent (6 ml) with alcohols (0.3 mmol) was degassed and saturated with O$_2$ before the photocatalytic reaction. The reaction was performed for 40 h under the irradiation of a white light LED lamps of 5.0 W power (PCX50A Discover reaction system, Beijing Perfectlight Co. Ltd. λ = 420–780 nm, power density ≈ 150 mW/cm^2) and the photo of the photocatalytic reaction system is offered in supporting information. The catalytic results were
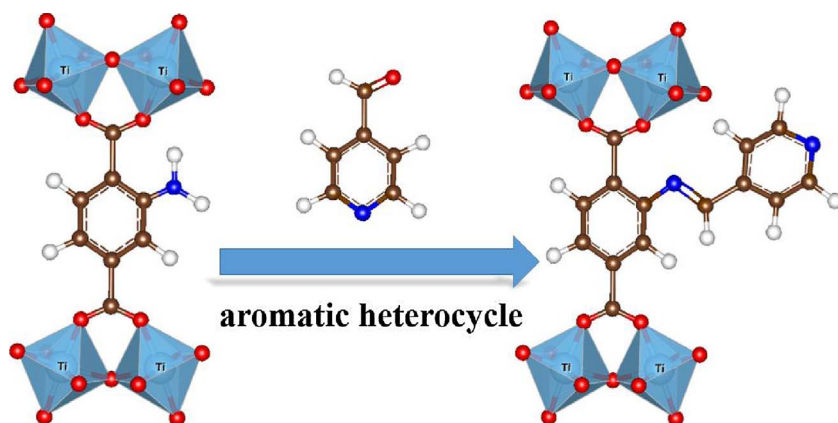
Scheme 1. Post-synthetic strategy of grafting NH$_2$-MIL-125(Ti) with aromatic heterocycles.

aromatic heterocycle

analyzed by a gas chromatography-mass spectrum (GC–MS, Agilent 7890/5975C-GC/MSD) with HP5-MS column. The yield was evaluated by using nitrobenzene as the internal standard.

3. Results and discussion

The XRD patterns of NH$_2$-MIL-125(Ti) and heterocycle-grafted NH$_2$-MIL-125(Ti) MOFs were shown in Fig. 1, which is in good agreement with simulated XRD patterns of NH$_2$-MIL-125(Ti) reported by the Ḟerey group [33]. The heterocycle-grafted MOFs showed that the crystal structure has not changed significantly, indicating that they still maintained the original skeleton structure and crystal morphology. The modification by these aldehyde groups is only a simple chemical connection and it does not affect the crystal structure of MOFs, implying that the catalytic materials have good chemical stability, thus the heterocycle-grafted materials can both maintain the structure of aromatic heterocycles and the MOFs structure.

Since the analysis of XRD cannot demonstrate that MOFs were successfully grafted and the analysis of the fingerprint region did not provide a direct proof of the formation of the Schiff base. In order to confirm the designed modification, the MOFs grafted by aromatic heterocycles were dissolved in DMSO-d^6 and analyzed by ^{1}H NMR spectroscopy. The ^{1}H NMR patterns for QUI-MIL-125(Ti) was elaborated in Fig. 2 and others were exhibited in Figs. S1–S4. Digested NH$_2$-MIL-125(Ti) shows mainly two sets of doublet-peaks and one singlet proton peak, which correspond to the three aromatic protons. The triangle symbol belonged to the pristine hydrogen atom on the o-position of the amino-functional group, the circular symbol belonged to the modified MOFs on the same position. The hydrogen atom marked as triangle was influenced by aromatic hetero-cycles, resulting in the atom in the different condition compared with primary MOF [35]. The modification ratio was measured by integration of ^{1}H NMR pattern, and it showed that the amount of modification was among 16–18%. The conjugated structure by Schiff base reaction was also measured and proved by FT-IR (Fig. 3). At the wavenumber of 1200 cm^{-1} to 1650 cm^{-1}, the peaks of QUI-MIL-125(Ti) compared with the original NH$_2$-MIL-125(Ti) remained essentially unchanged, suggesting that QUI-MIL-125(Ti) re-

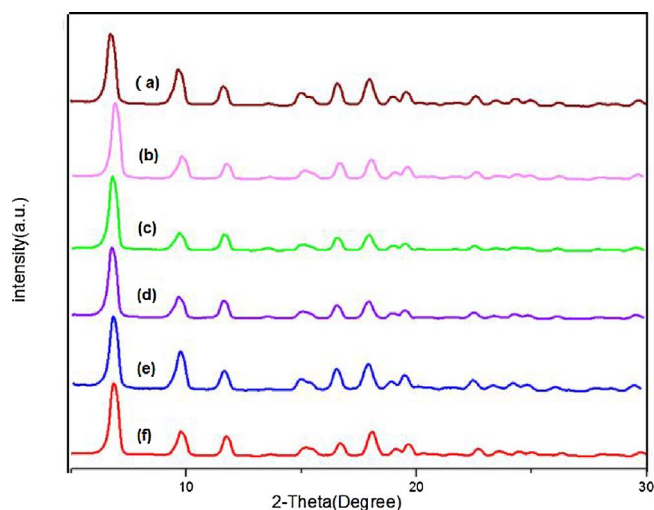**Fig. 1.** Powder XRD patterns of different samples:(a) NH$_2$-MIL-125(Ti), (b) THI-MIL-125(Ti), (c) QUI-MIL-125(Ti), (d) 2-PA-MIL-125(Ti), (e) 3-PA-MIL-125(Ti), (f) 4-PA-MIL-125(Ti).
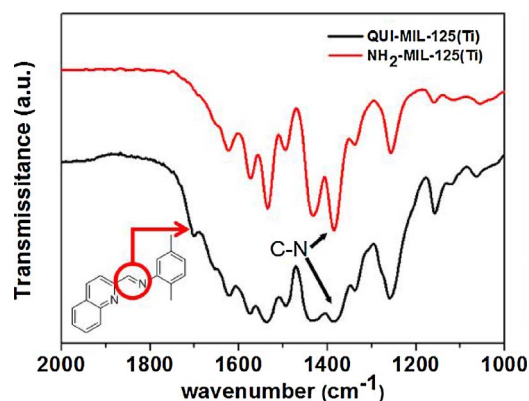

Fig. 3. FT-IR of QUI-MIL-125(Ti) and NH$_2$-MIL-125(Ti). The peak at 1700 cm^{-1} (black line) belongs to the region of Schiff base.
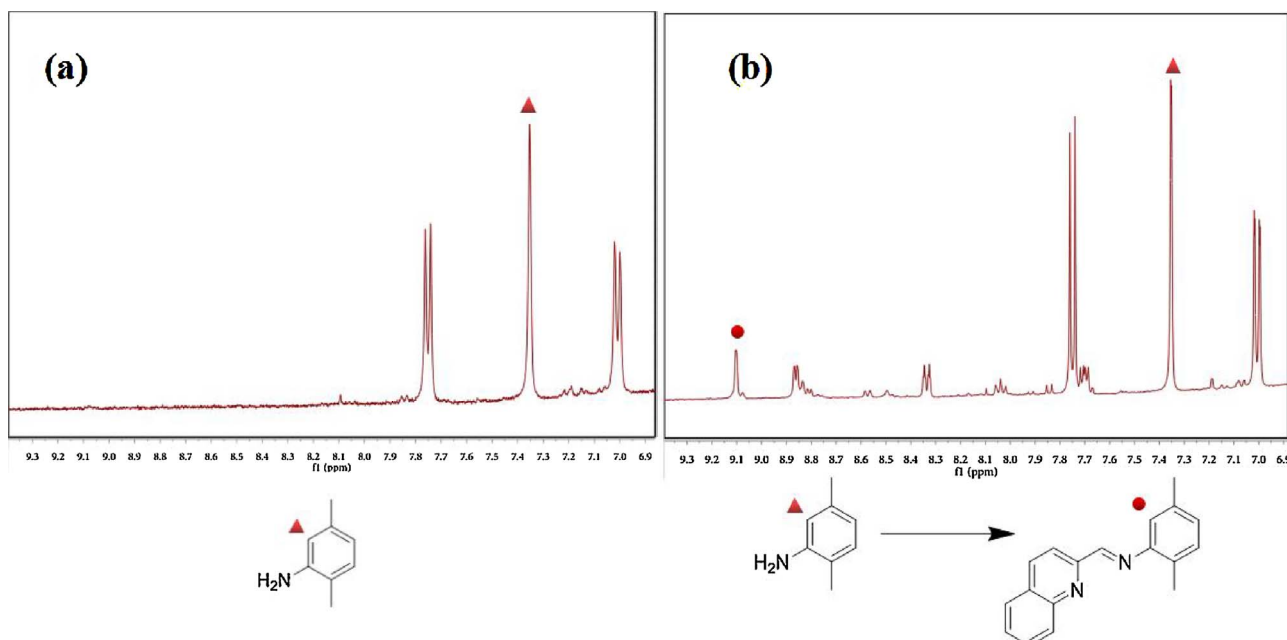

Fig. 2. (a) ^{1}H NMR patterns for NH$_2$-MIL-125(Ti). (b) ^{1}H NMR patterns for QUI-MIL-125(Ti). The triangle symbol belonged to the pristine hydrogen atom on the o-position of the amino-functional group and the circular symbol belonged to the aromatic heterocycle-grafted MOFs.
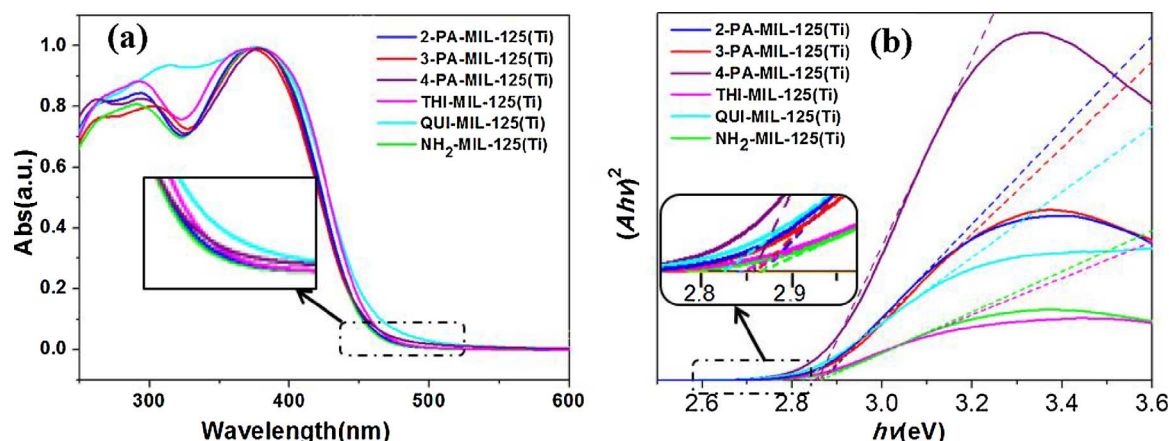
Fig. 4. (a) UV–vis DRS spectra of NH_2-MIL-125 and aromatic heterocycle-grafted NH_2-MIL-125 (b) plots of $(Ah\nu)^2$ as a function of *vs.* Photon energy of NH_2-MIL-125 and aromatic heterocycle-grafted NH_2-MIL-125.

tained $-NH_2$ chemical bond. A new peak appeared at the wavenumber of 1700 cm^{-1}, which was consistent with the region of Schiff base. The peak at 1360 cm^{-1} was the absorption peak of the chemical bond between the carbon atom connected with the benzene ring and the nitrogen atom in the amino group. After the post-grafting, the absorption peak at 1360 cm^{-1} was weakened due to the change of $-NH_2$ which the C–N chemical bond was adjacent to, indicating the successful modification of aromatic heterocycles via Schiff base reaction with $-NH_2$ group in NH_2-MIL-125(Ti).

In the process of post-grafting, the reaction was controlled under the same environment. The molar ratio of aromatic heterocycles and MOFs was limited at 1:2, and the reaction was proceeded at 70 °C for 3 days. The reaction was basically balanced, and the post-synthetic modification of aromatic heterocycles in all MOFs would be in a relatively close range to allow for better experimental comparisons.

In order to explore the enhanced photocatalytic effect in aromatic heterocycle-grafted NH_2-MIL-125(Ti) MOFs, we performed a combined experimental and computational study to elucidate the structure of NH_2-MIL-125(Ti) and the impact of aromatic heterocycles on the NH_2-BDC (2-aminoterephthalic acid) linker. It was confirmed that NH_2-MIL-125(Ti) was subjected to a series of aromatic heterocycles by targeted synthesis. Optical absorption of the different materials was investigated by using UV–vis spectroscopy. The calculation of the band gap is predicted by density functional theory (DFT). Optical responses of the as-prepared photocatalysts were conducted on a UV–vis DRS. The heterocycle-grafted NH_2-MIL-125(Ti) MOFs mainly exhibit two absorption bands at 290 and 390 nm which were attributed to $ATA^{2-}Ti^{4+} \rightarrow ATA^-Ti^{3+}$ transition within the subunits of the framework [36,37]. The absorption wavelength of NH_2-MIL-125(Ti) showed red shift after modified with aromatic heterocycles (Fig. 4a). QUI-MIL-125(Ti) and THI-MIL-125(Ti) exhibited much better light absorption enhancement which can be associated with a higher level of conjugation of the aromatic system. After the introduction of aromatic heterocycles in MOFs, the amino groups and aldehydes on the ligands form the structure of Schiff base. This structure would lead to a super-conjugation effect with the benzene ring in NH_2-MIL-125(Ti) and aromatic heterocycles, which is favorable for the charge excitation and transition in the photocatalytic reaction. The intercept of the tangents of $(Ah\nu)^2$ *vs.* photon energy was used to estimate the band-gap energy (Fig. 4b). The samples demonstrated similar band gaps of ∼2.85 eV (Table S1 in the SI). The calculated band gap energies were found to be 2.88 eV for NH_2-MIL-125(Ti), which was larger than those of the heterocycle-grafted NH_2-MIL-125(Ti) MOFs, so that the introduction of aromatic heterocycles reduced the band gap of MOFs and had a better response for visible light.

PL spectroscopy was executed with an excitation wavelength of

300 nm to further elucidate the optical response of heterocycle-grafted MOFs. The PL spectra (Fig. 5a) of NH_2-MIL-125(Ti) showed the strongest intensity, indicating that it had the lowest recombination rate of photoexcited electrons under an excitation at 300 nm. The intensity of QUI-MIL-125(Ti) is lower than that of other heterocycle-grafted MOFs and the result corresponds to the UV–vis DRS. The nitrogen adsorption-desorption isotherms curves in Fig. 5b for NH_2-MIL-125(Ti) and its modified products exhibited type I isotherm. The BET specific surface area of NH_2-MIL-125(Ti) in Table 1 was only slightly lower than that reported previously, indicating that NH_2-MIL-125(Ti) with good quality was obtained [33]. Compared with the original NH_2-MIL-125(Ti), the heterocycle-grafted MOFs had a different degree of decrease in specific surface area and pore volume, and there was no obvious change for the pore size. It can be clarified that the aromatic heterocycles occupy a portion of the pore volume.

To determine the exact band gap edges of heterocycle-grafted NH_2-MIL-125(Ti) MOFs, their Mott-Schottky plots (Fig. 6a) and XPS valence band spectra (Fig. 6b) were analyzed. The plots of heterocycle-grafted MOFs exhibited positive slopes at 2 kHz. This is a typical characteristic of n-type semiconductors. The flat band potentials derived from the x-intercept in the Mott–Schottky plots of heterocycle-grafted MOFs were −1.07 V versus the saturated Ag/AgCl reference electrode (pH = 7), respectively. The conduction band (CB) potential is very close to the flat band potential in n-type semiconductors. Moreover, the XPS valence band spectra showed that the extrapolated dominant edges of valence band of aromatic heterocycle-grafted MOFs exhibited obvious shift compared with NH_2-MIL-125(Ti). The conduction band (CB) and valence band (VB) potential of heterocycle-grafted MOFs can be calculated using the equation related to Mulliken electronegativity and the band gap of semiconductor [34]:

$$E_{VB} = X - E^e + 0.5\ E_g$$

Table 1
BET surface area of aromatic heterocycle-grafted NH_2-MIL-125(Ti).

Sample	S_{BET} (m^{2}g^{-1}) [a]	V_{pore} (cm^{3}g^{-1}) [b]	Pore size (nm) [c]
NH_2-MIL-125(Ti)	1176.1	0.46	2.23
2-PA-MIL-125(Ti)	826.8	0.31	2.17
3-PA-MIL-125(Ti)	979.0	0.38	2.21
4-PA-MIL-125(Ti)	881.9	0.39	2.17
QUI-MIL-125(Ti)	823.4	0.31	2.17
THI-MIL-125(Ti)	925.2	0.33	2.14

[a] Calculated by the BET method.
[b] Accumulated pore volume from the N_2 adsorption branch with P/P_0 lower than 0.997.
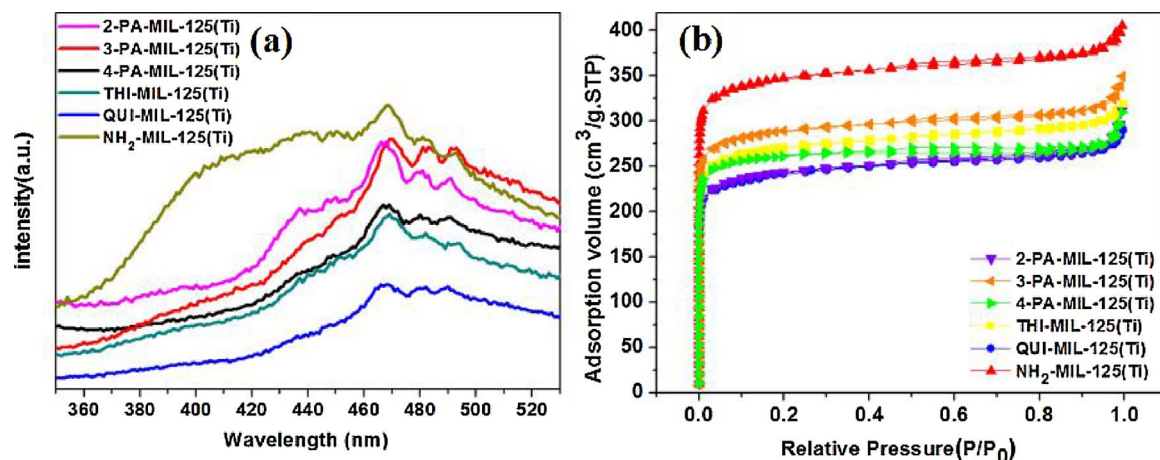[c] Obtained from the N_2 adsorption branch by the BJH method.

Fig. 5. (a) PL spectra of aromatic heterocycle-grafted MOF with an excitation wavelength of 300 nm. (b) N_2 adsorption-desorption isotherms of aromatic heterocycle-grafted NH_2-MIL-125(Ti).

Where E_{VB} and E_g are the bottom position of VB relative to the *NHE* level and band gap of the semiconductor, respectively, and X is the geometric mean of Mulliken electronegativity of the constituent atoms in the semiconductor, E^e is the energy of free electrons on the hydrogen scale. The calculated VB is listed in Table S2.

In order to further understand the effect of post-grafting on MOFs photocatalysts, electronic structure calculations on the same series of heterocycle-grafted NH_2-MIL-125(Ti) solids were performed using Density functional theory (DFT). The structural calculations of aromatic heterocycle-grafted MOFs were computed at the DFT-HSE06 level of

theory, a form of the general gradient approximation (GGA), with basis set 6–31G*. Specially, the bottom atoms were frozen at fired position during the optimization processes. Since aromatic heterocycle-grafted NH_2-MIL-125(Ti) is a substance with the same continuous unit [37,38], some of the representative molecules can be selected as the target of computational simulation. Fig. 7a–f depicted the valence band (VB) and conduction band (CB) orbitals. The CB, VB corresponds to LUMO, HOMO, respectively. The upper VB is composed of C 2p orbital within NH_2-BDC and aromatic heterocycles, the introduction of aromatic heterocycles splits the VB into a high energy occupied state (depicted in
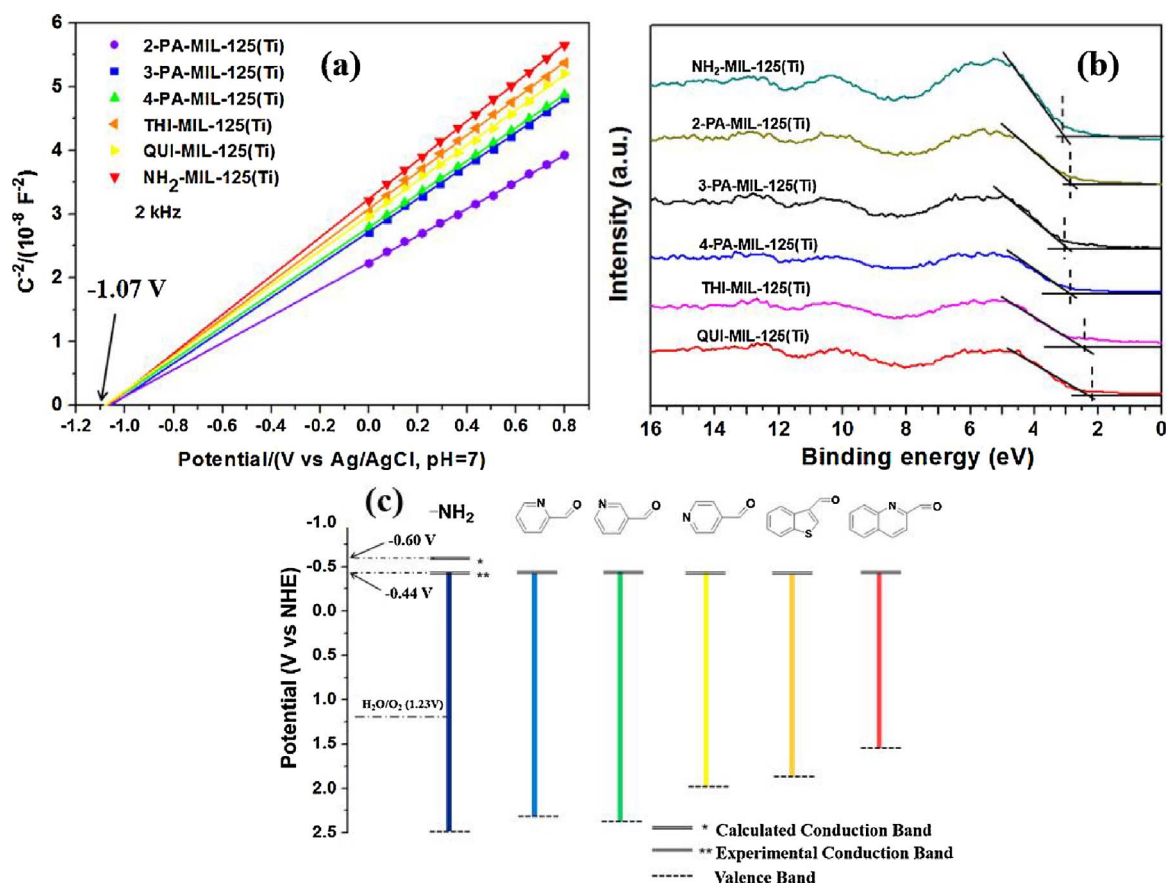

Fig. 6. (a) Typical Mott-Schottky plots of aromatic heterocycle-grafted NH_2-MIL-125(Ti). (b) XPS valence band spectra of aromatic heterocycle-grafted NH_2-MIL-125(Ti). (c) Band gap of series of aromatic heterocycle-grafted NH_2-MIL-125(Ti), the band gap varied when the aromatic heterocycles is changed. Quinoline-2-carbaldehyde and thiophene-3-carbaldehyde achieved narrower band gap comparing with the x-pa. (x = 1, 2, 3) and NH_2-MIL-125(Ti).
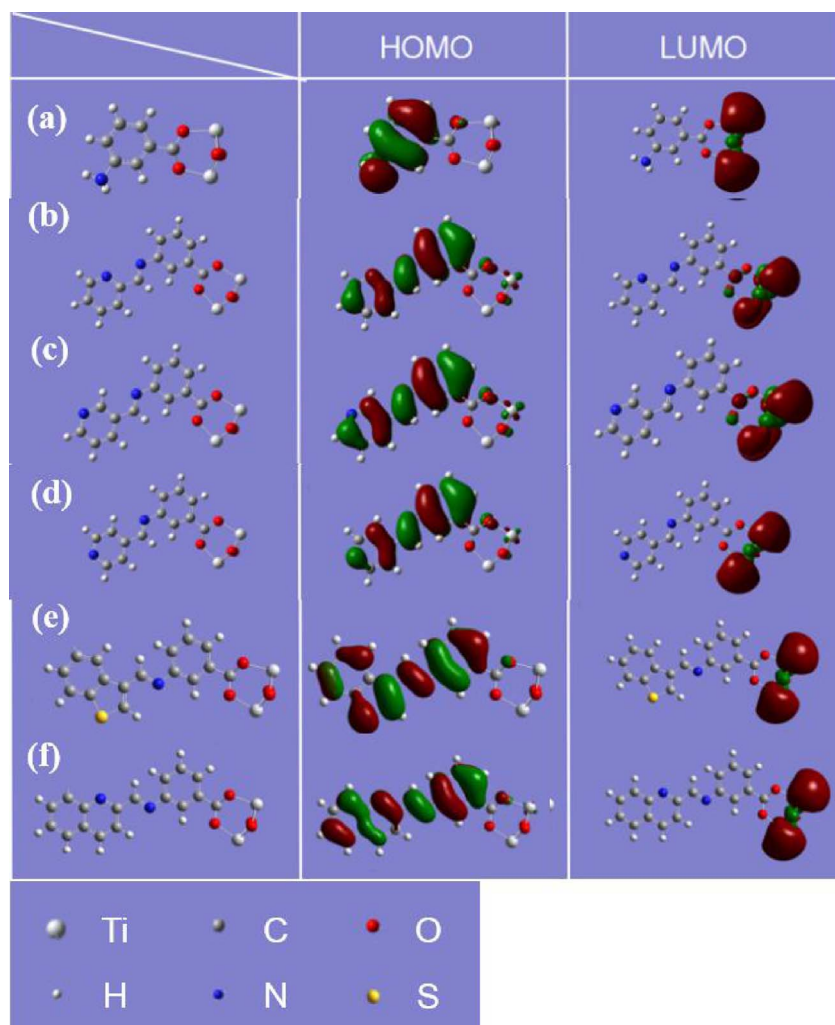
Fig. 7. Simulated model of aromatic heterocycle-grafted MOF: (a) NH$_2$-MIL-125(Ti), (b) 2-PA-MIL-125(Ti), (c) 3-PA-MIL-125(Ti), (d) 4-PA-MIL-125(Ti), (e) THI-MIL-125(Ti), (f) QUI-MIL-125(Ti). The VB is composed of the C 2p orbitals (shown on the middle). The modification of aldehydes on NH$_2$-MIL-125 makes the conjugation effect on NH$_2$-BDC further increase. The CB is composed of O 2p orbitals and Ti 3d orbitals (shown on the bottom), suggesting that modifications of the amino group units are unlikely to affect the LUMO.

Fig. 6b). The CB is composed of O 2p orbitals and Ti 3d orbitals, so that grafting with the aromatic heterocycle units is unlikely to affect the CB. It was also proved by the results of Mott–Schottky plots of grafted MOFs, the plots converged at one point, suggesting the same position of CB. Theoretical [40] and experimental data of VB is depicted in Fig. 6b. The shape of the electron cloud in Fig. 7 can also assist in providing the evidence. Due to the role of modification, the conjugate effect is further expanded and modified aromatic heterocycles also have strong electron-donating characteristics which result in lower band gaps in the grafted MOFs. Moreover, 2-PA and 3-PA are weakly electron-donating or withdrawing. The 4-PA aromatic heterocycle has better performance in electron-donation compared with 2-PA and 3-PA, which is also reflected in the predicted band gap of 2.6 eV of 4-PA-MIL-125(Ti). And QUI and THI show best electron-donating within the aromatic heterocycles due to the introduction of benzene ring and sulfur-like heteroatoms in aromatic heterocycles. The conjugate effect within QUI-MIL-125(Ti) due to the interaction of the electron cloud (red and green area in Fig. 7f) is stronger than that of THI-MIL-125(Ti) and other grafted MOFs, indicating that QUI-MIL-125(Ti) has a lower band gap and could improve the optical absorption.

We obtained the band gaps of heterocycle-grafted MOFs by simulating the structure and calculating the HOMO and LUMO. In the process of synthetic modification, not all of the amino groups reacted with the aromatic heterocycles. Thus there are some difference between the band gaps calculated by DFT and the actual band gaps of modified MOFs. In order to approximate the actual band gaps of heterocycle-grafted MOFs, the exact amount of modification was obtained by [1]H

NMR analysis. From the result of integrals, the amount of modification was about 17%. It can be inferred that the amount of NH$_2$-MIL-125(Ti) was about 83%. So the actual band gap of heterocycle-grafted MOFs consisted of 83% NH$_2$-MIL-125(Ti) and 17% heterocycle-grafted MOFs. The computational approach predicted a band gap of 2.806 eV for QUI-MIL-125(Ti), which is close to 2.832 eV measured from UV–vis optical absorption analysis. The relative error factor was calculated and it was within 3.5%. The details of calculation results were listed in Table S3.

Benzyl alcohol was chosen as the reaction substrate to demonstrate the effect of the aromatic heterocycle grafting of NH$_2$-MIL-125(Ti) on the photocatalytic performance under visible light. First, the heterocycle-grafted MOFs were activated under 150 °C for 3 h then the reaction was carried out under room temperature by using 30 mg modified MOFs along with 1 atm of molecular oxygen as the oxidant and 6 ml acetonitrile as the solvent. After the reaction was conducted for 40 h, benzyl alcohol was converted to benzaldehyde with a good yield (88%) and high selectivity (> 99%) (Table 2, Entry 1) with the catalyst of QUI-MIL-125(Ti). THI-MIL-125(Ti) also has a good photocatalytic performance, which converted 86% benzyl alcohol into benzaldehyde (Table 2, Entry 2). 4-PA-MIL-125(Ti) has a similar catalytic efficiency with 3-PA-MIL-125(Ti), 2-PA-MIL-125(Ti), and the conversion of benzyl alcohol is more than 79% (Table 2, Entries 3–5). We also designed the contrast test, proving that small molecules aldehydes does not improve the photocatalytic performance of NH$_2$-MIL-125(Ti), only through chemical bond connection can really improve the photocatalytic ability of NH$_2$-MIL-125(Ti), as shown in Table 2 Entries 6–11. In addition, QUI-MIL-125(Ti) didn't show any activity under dark

Table 2
Photocatalytic oxidation of benzyl alcohol with different catalysts.[a]

Entry	Cat.	Conv. (%)[b]	Select. (%)[b]
1	QUI-MIL-125(Ti)	88	> 99
2	THI-MIL-125(Ti)	86	> 99
3	4-PA-MIL-125(Ti)	82	> 99
4	3-PA-MIL-125(Ti)	79	> 99
5	2-PA-MIL-125(Ti)	79	> 99
6	NH₂-MIL-125(Ti)	69	> 99
7	NH₂-MIL−125(Ti)+QUI[c]	69	> 99
8	NH₂-MIL−125(Ti)+THI[c]	69	> 99
9	NH₂-MIL−125(Ti)+4-PA[c]	69	> 99
10	NH₂-MIL−125(Ti)+3-PA[c]	69	> 99
11	NH₂-MIL−125(Ti)+2-PA[c]	69	> 99
12	QUI-MIL−125(Ti)[d]	–	–
13	QUI-MIL−125(Ti)[e]	–	–

[a] Reaction conditions: Photocatalysts: 30 mg, MeCN: 6 ml, benzyl alcohol: 0.3 mmol. The solutions were irradiated by white-light LED lamps with the light in the range of 420–780 nm for 40 h at room Temperature under 1 atm O_2.

[b] Conversion and selectivity were determined by GC/MS using nitrobenzene as internal standard.

[c] QUI: 2-quinolinecarboxaldehyde, THI: 3-thiophenecarboxaldehyde, 4-PA: 4-pyridinecarboxaldehyde, 3-PA: 3-pyridinecarboxaldehyde, 2-PA: 2-pyridinecarboxaldehyde Photocatalysts: 30 mg NH₂-MIL-125(Ti) and 1 mg aromatic hetero-cycles, the other catalyst condition is the same as entries 1–6.

[d] The reaction is under the dark condition under 1 atm O_2.

[e] The reaction is under 1 atm pure Ar atmosphere.

condition or under 1 atm Ar atmosphere, as shown in Entries 12 and 13 of Table 2, indicating the visible light and the oxygen gas are essential for the photocatalytic oxidation of alcohols.

Under the same conditions, the photocatalytic reaction of different alcohols was carried out by QUI-MIL-125(Ti). The reaction results are shown in Table 3. Under the influence of electron-donating groups, the conversions of alcohols substituted by CH_3O- or CH_3- were higher than

Table 3
Photocatalytic oxidation of various substituted alcohols over QUI-MIL-125(Ti).

[a]Entry	Substrate	Product	[b]Conv. (%)	[c]Selec. (%)
1	benzyl alcohol	benzaldehyde	88	> 99
2	2-methylbenzyl alcohol	2-methylbenzaldehyde	90	> 99
3	4-methylbenzyl alcohol	4-methylbenzaldehyde	93	> 99
4	4-methoxybenzyl alcohol	4-methoxybenzaldehyde	> 99	> 99
5	4-nitrobenzyl alcohol	4-nitrobenzaldehyde	47	> 99
6	4-fluorobenzyl alcohol	4-fluorobenzaldehyde	71	> 99
7	diphenylmethanol	benzophenone	52	> 99
8	α-methylbenzyl alcohol	acetophenone	46	> 99

[a] Reaction conditions: Photocatalysts: 30 mg, MeCN: 6 ml, substrate: 0.3 mmol, visible-light irradiation (420–780 nm), 1 atm O_2, 40 h.

[b] Conversation of the alcohols calculated by GC analysis.

[c] Selectivity of the aldehydes or ketones.

that of benzyl alcohol (Table 3, Entries 1–4). Due to the introduction of electron-donating groups, the electron cloud density of the aromatic alcohol increases and alcohol's electrons are easier to be taken away, resulting in higher conversion of alcohols substituted by CH_3O- and CH_3-. In addition, the better electron-donating effect of CH_3O- than that of CH_3- results in a higher conversion of photocatalytic conversion of substituted alcohols. While in the cases of those with electron-withdrawing groups (e.g., F- and NO_2-), the conversion of alcohols to the corresponding aldehydes was lower than that of benzyl alcohol (Table 3, Entries 5, 6) and substrates with higher electron-withdrawing group (i.e., NO_2-) showed worse performance (i.e., 47% conversion) than that (i.e., 71% conversion) with lower electron-withdrawing group (e.g., F-). In addition, the secondary alcohols such as diphenylmethanol α-Methylbenzyl alcohol (Table 3 Entries 7, 8) were tested as a typical secondary alcohol and much lower activity was observed. The hydrogen atoms associated with the secondary alcohol are reduced. In the process of de-protonation, hydrogen is more difficult to be removed to form carbon centered radicals. So the secondary alcohol is more difficult to be oxidized.

QUI-MIL-125(Ti) was selected as catalyst to show their reversibility. After each cycle, it was separated by centrifugation, washed with ethanol for several times and dried in a 60 °C oven for 16 h. The experimental results exhibited that there is no obvious change in photocatalytic activity after repeated cycles. Because the post-grafting of NH₂-MIL-125(Ti) is linked by molecular bonds, and the molecular bonds are less likely to break apart after the reaction. Therefore, QUI-MIL-125(Ti) can maintain a good catalytic conversion rate and
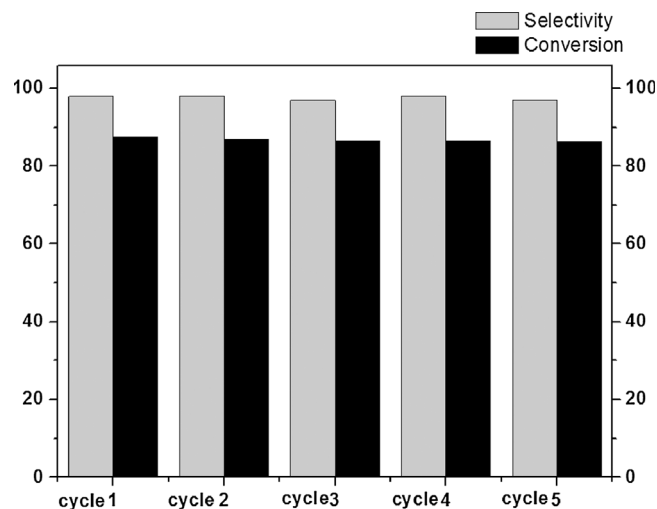

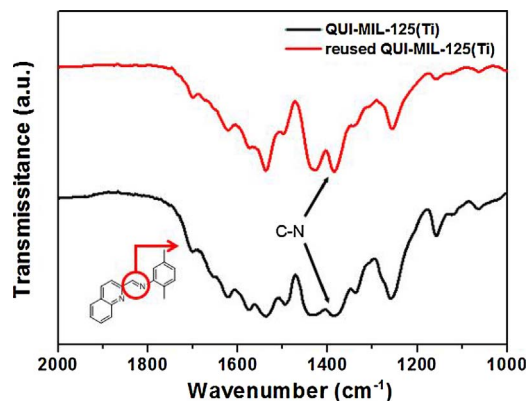**Fig. 8.** The recyclability of QUI-MIL-125(Ti) catalyst in the oxidation of benzyl alcohol.

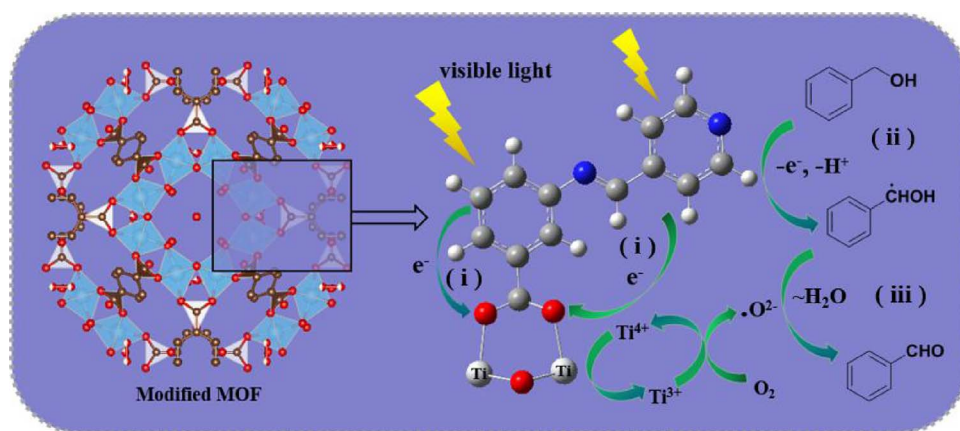**Fig. 9.** FT-IR of QUI-MIL-125(Ti) and reused QUI-MIL-125(Ti).

Fig. 10. Proposed mechanism of the photocatalytic benzyl alcohols oxidation over aromatic heterocycle-grafted NH$_2$-MIL-125(Ti).

selectivity (Fig. 8). The catalyst maintained more than 85% conversion of benzyl alcohol and 99% selectivity of benzaldehyde after five runs. The FT-IR spectra of photocatalysts after the five runs was provided in Fig. 9. The peak of Schiff base is still appeared at the wavenumber of 1700 cm^{-1}. And the absorption peak at 1360 cm^{-1} was still weakened as origin QUI-MIL-125(Ti).

There is no activity observed when the photocatalytic reaction under pure Ar using QUI-MIL-125(Ti) as photocatalyst was carried out. And it can be inferred that in the process of aerobic oxidation of benzyl alcohol, the in-situ formed super-oxide radical anion ($\cdot O^{2-}$) plays an important role [41]. Upon irradiations, an electron can be transferred from the excited ligand ATA to Ti-O oxo-clusters to form Ti^{3+} moiety (step i in Fig. 10). The as-formed Ti^{3+} can react with molecular oxygen to generate $\cdot O^{2-}$ while Ti^{3+} is oxidized back to Ti^{4+} (Fig. 10). The experiment results indicated that electron-donating groups showed better performance than those with electron-withdrawing groups, substrates with higher electron-donating groups (CH$_3$O-) showed better performance than those with lower electron-donating groups (CH$_3$-). So it can be concluded a proposed process in the whole mechanism, where benzyl alcohol can donate an electron, followed by a de-protonation process to generate the carbon centered radical (step ii in Fig. 10). The interaction between the photo-generated carbon centered radical and the $\cdot O^{2-}$ will lead to the formation of aldehydes (step iii in Fig. 10). The introduction of aromatic heterocycles developed a lower band gap of NH$_2$-MIL-125(Ti). And there are more electron-hole pairs involved in the surface reaction. As a result, more electrons can be transferred from benzyl alcohol to Ti-O oxo-clusters and it actually accelerates the reaction process of step i and step ii. In this process more benzyl methanol radicals and $\cdot O^{2-}$ have been formed and it results in higher conversion of benzyl alcohol.

4. Conclusions

Based on Schiff base reaction, the improved conjugated system has been developed to fabricate novel aromatic heterocycle-modified NH$_2$-MIL-125(Ti) MOFs. The introduction of aromatics, especially 2-quinolinecarboxaldehyde and 3-thiophenecarboxaldehyde, enables the modification of the intrinsic electronic properties, and enhancement of the visible light response of NH$_2$-MIL-125(Ti). DFT calculations showed that the optical response of aromatic heterocycle-modified NH$_2$-MIL-125(Ti) expanded the absorption in the visible light region. Hence the as-obtained MOF showed substantially enhanced photocatalytic in aerobic oxidation of benzyl alcohols compared with that of the pristine NH$_2$-MIL-125(Ti). Through this facile strategy, large numbers of aromatics can be grafted onto NH$_2$-MIL-125(Ti). We anticipate that this post-modification strategy will provide novel routes to construct MOFs with reduced structural defects and improved photo-catalytic activities.

Appendix A. Supplementary data

Supplementary data associated with this article can be found, in the online version, at http://dx.doi.org/10.1016/j.apcatb.2017.10.034.

References

[1] J.L.C. Rowsel, O.M. Yaghi, Microporous Mesoporous Mater. 73 (2004) 3–14.
[2] T.R. Cook, Y.R. Zheng, P.J. Stang, Chem. Rev. 113 (2013) 734–777.
[3] J.R. Li, J. Sculley, H.C. Zhou, Chem. Rev. 112 (2012) 869–932.
[4] A. Corma, H. García, F.X.L. i Xamena, Chem. Rev. 110 (2010) 4606–4655.
[5] P. Horcajada, R. Gref, T. Baati, P.K. Allan, G. Maurin, P. Couvreur, G. Férey, R.E. Morris, C. Serre, Chem. Rev. 112 (2012) 1232–1268.
[6] G. Férey, Chem. Soc. Rev. 37 (2008) 191–214.
[7] L.J. Murray, M. Dinca, J.R. Long, Chem. Soc. Rev. 38 (2009) 1294–1314.
[8] L. Ma, C. Abney, W. Lin, Chem. Soc. Rev. 38 (2009) 1248–1256.
[9] W. Xuan, C. Ye, M. Zhang, Z. Chen, Y. Cui, Chem. Sci. 4 (2013) 3154–3159.
[10] A. Sclafani, L. Palmisano, G. Farneti, Chem. Commun. 6 (1997) 529–530.
[11] T. Tachikawa, J.R. Choi, M. Fujitsuka, T. Majima, J. Phys. Chem. C 112 (2008) 14090–14101.
[12] M. Alvaro, E. Carbonell, B. Ferrer, F.X.L. Xamena, Chem. Eur. J. 13 (2007) 5106–5112.
[13] C.K. Lin, D. Zhao, W.Y. Gao, Z.Z. Yang, J.Y. Ye, T. Xu, Q.F. Ge, S.Q. Ma, D.J. Liu, Inorg. Chem. 51 (2012) 9039–9044.
[14] J.L. Wang, C. Wang, W. Lin, ACS Catal. 2 (2012) 2630–2640.
[15] C.G. Silva, I. Luz, F.X. Llabrés i Xamena, A. Corma, H. García, Chem. Eur. J. 16 (2010) 11133–11138.
[16] C. Wang, Z. Xie, K.E. Dekrafft, W. Lin, J. Am. Chem. Soc. 133 (2011) 13445–13454.
[17] D.I. Enache, J.K. Edwards, P. Landon, B. Solsona-Espriu, A.F. Carley, A.A. Herzing, M. Watanabe, C.J. Kiely, D.W. Knight, G.J. Hutchings, Science 311 (2006) 362–365.
[18] F. Arena, B. Gumina, C. Cannilla, L. Spadaro, A. Patti, L. Spiccia, Appl. Catal. B-Environ. 170–171 (2015) 233–240.
[19] K. Leus, Y.Y. Liu, P. Van Der Voort, Catal. Rev. Sci. Eng. 56 (2014) 1–56.
[20] M.B. Chambers, X. Wang, N. Elgrishi, C.H. Hendon, A. Walsh, J. Bonnefoy, J. Canivet, E.A. Quadrelli, D. Farrusseng, C. Mellot-Draznieks, M. Fontecave, ChemSusChem 8 (2015) 603–608.
[21] J.G. Nguyen, S.M. Cohen, J. Am. Chem. Soc. 132 (2010) 4560–4561.
[22] K.K. Tanabe, S.M. Cohen, Angew. Chem. 48 (2009) 7424–7427.
[23] N.A. Maxim, G.G. Maarten, S.J. Tom, K. Freek, G. Jorge, Chem. Commun. 49 (2013) 10575–10577.
[24] X. Li, Y. Pi, Q. Xia, Z. Li, J. Xiao, Appl. Catal. B-Environ. 191 (2016) 192–201.
[25] J. Zhang, Y. Chen, X. Wang, Energy Environ. Sci. 8 (2015) 3092.
[26] J. Qin, S. Wang, H. Ren, Y. Hou, X. Wang, Appl. Catal. B-Environ. 179 (2015) 1–8.
[27] J. Zhang, M. Zhang, S. Lin, X. Fu, X. Wang, J. Catal. 310 (2014) 24.
[28] G. Zhao, H. Pang, G. Liu, P. Liu, H. Liu, H. Zhang, L. Shi, J. Ye, Appl. Catal. B-Environ. 200 (2017) 141–149.
[29] J.J. Tian, L. Zhang, X.Q. Fan, Y. Zhou, M. Wang, R. Cheng, M. Li, X.T. Kan, X.X. Jin, Z.H. Liu, Y.F. Gao, J.L. Shi, J. Mater. Chem. A 4 (2016) 13814.
[30] J. Tang, W. Dong, G. Wang, Y.Z. Yao, L.M. Cai, Y. Liu, X. Zhao, J.Q. Xu, L. Tan, RSC Adv. 4 (2014) 42977.
[31] C.J. Doonan, W. Morris, H. Furukawa, O.M. Yaghi, J. Am. Chem. Soc. 131 (2009)

9492–9493.

[32] Y. Zhang, Y. Chen, Y. Zhang, H. Cong, B. Fu, S.P. Wen, S.P. Ruan, J. Nanopart. Res. 15 (2013) 2014.

[33] C. Zlotea, D. Phanon, M. Mazaj, D. Heurtaux, V. Guillerm, C. Serre, P. Horcajada, T. Devic, E. Magnier, F. Cuevas, G. Ferey, P.L. Llewellyn, M. Latroche, Dalton Trans. 40 (2011) 4879–4881.

[34] Z. Li, X. Chen, Z. Xue, Sci. Chi. Chem. 56 (2013) 443–450.

[35] Y. Luan, Y. Qi, H.Y. Gao, R.S. Andriamitantsoa, N.N. Zheng, G. Wang, J. Mater. Chem. A 3 (2015) 17320–17331.

[36] J. Gascon, M.D. Herna'ndez-Alonso, A.R. Almeida, G.P. van Klink, F. Kapteijn, G. Mul, ChemSusChem 1 (2008) 981–983.

[37] H. Khajavi, J. Gascon, J.M. Schins, L.D.A. Siebbeles, F. Kapteijn, J. Phys. Chem. C 115 (2011) 12487–12493.

[38] C.G. Hendon, D. Tiana, M. Fontecave, C. Sanchez, L. D'arras, C. Sassoye, L. Rozes, C. Mellot-Drznieks, A. Walsh, J. Am. Chem. Soc. 135 (2013) 10492–10945.

[40] K.T. Butler, C.H. Hendon, A. Walsh, J. Am. Chem. Soc. 136 (2014) 2703–2706.

[41] D.R. Sun, L. Ye, Z.H. Li, Appl. Catal. B-Environ. 164 (2015) 428–432.